Journal of the European Ceramic Society 18 (1998) 1893–1904

PII: S0955-2219(98)00128-9
0955-2219/98/$—see front matter

Si_3N_4/SiCN Nanocomposites: Influence of SiC Nanoprecipitates on the Creep Behaviour

J.-L. Besson,[a]* M. Mayne,[b] D. Bahloul-Hourlier[b] and P. Goursat[b]

[a]LMCTS, ESA CNRS 6015, ENSCI, 47 Av. A. Thomas, 87065 Limoges, France
[b]LMCTS, ESA CNRS 6015, Université de Limoges, 123 Av. A, Thomas, 87060 Limoges, France

Abstract

The compressive creep behaviours of a silicon nitride ceramic densified with yttria and alumina and of the same material containing 10 wt% SiC nanoparticles are compared in the 1250–1450°C temperature range under stresses ranging from 45 to 180 MPa. The stress exponents are ~0·8 and 1 and the apparent activation energies are 514 and 590 kJ mol^{-1} for the monolith and the composite, respectively. No signs of cavitation are observed. For both materials grain boundary sliding accommodated by diffusion through the intergranular glass phase is considered as the primary steady-state creep mechanism. The higher creep resistance of the composite is connected to the presence of intergranular SiC nanoparticles which limit grain boundary sliding and to the difference in chemical composition of the intergranular glass phase.

Les comportements au fluage d'une céramique de type nitrure de silicium densifiée avec de l'yttrine et de l'alumine et du même matériau contenant 10% en masse de nanoparticules de SiC sont comparés dans le domaine de température 1250–1450°C sous des contraintes variant de 45 à 180 MPa. Les exposants de contrainte valent respectivement ~0·8 et 1 et les énergies d'activation 514 et 590 kJ mol^{-1} pour le monolithe et le composite. Aucun signe de cavitation n'a été observé. Le glissement le long des joints de grains, accommodé par la diffusion à travers la phase vitreuse intergranulaire, est considéré comme le principal mécanisme agissant pendant le stade de fluage stationnaire. La résistance au fluage plus élevée du composite est reliée à la présence de nanoparticules de SiC en position intergranulaire, qui limitent le glissement le long des joints de grains, et à la difference de composition chimique des phases vitreuses intergranulaires. © *1998 Elsevier Science Limited. All rights reserved*

Keywords: silicon nitride, nanocomposites, creep

*To whom correspondence should be addressed.

1 Introduction

Silicon nitride based ceramics are the most promising candidates for structural applications at temperature higher than allowed by metallic superalloys. Nevertheless, potential applications were hindered by the difficulties of shaping these highly covalent materials until superplastic forming of Si_3N_4/SiC composites was demonstrated by Wakai and coworkers.[1,2] Recently, it was shown in our laboratory that an α-Si_3N_4 rich ceramic could be plastically deformed up to 80% elongation in tension.[3] However, tailoring a microstructure suitable for hot-forming (that is with a high ductility) must not sign away the resistance (in particular the creep resistance) at temperatures that must be significantly higher than the working temperature of metallic superalloys.

In this paper, we compare the creep behaviour in compression of the already mentioned α-Si_3N_4 rich ceramic with that of a Si_3N_4/SiC composite that could be deformed in tension up to 39% at 1595°C.

2 Materials and testing

2.1 Materials

The starting silicon nitride powder was the SNE 10 grade manufactured by UBE. It had a very high α-phase content (95 wt%). The Si_3N_4 particles, equiaxed in shape, were covered by a thin shell of a compound intermediate between silica and a silicon oxynitride.[4] The particle size ranged from 50 to 350 nm with a majority of them between 150 and 180 nm. The surface area was 15 m^2 g^{-1}. The impurity content was low ($\sum$[Al + Ca + Fe] = 600 ppm, C = 800 ppm). This powder was mixed in ethanol with 6 wt% Y_2O_3 (Rhône–Poulenc, 99·995% pure) and 3 wt% Al_2O_3 (Lonza, 99·99% pure) as sintering aids. Then, the dried mixture was hot-pressed for 2 h at 1550°C under 35 MPa using a BN coated graphite die operating in nitrogen. This rather low sintering temperature was selected as it led to nearly full

density ($\approx$ 99%) with a limited α to β-Si_3N_4 transformation.

The composite was fabricated by adding to the previous powder mixture nanosized SiCN powder synthesized by laser pyrolysis of a mixture of SiH_4 and CH_3NH_2 gases.[5] The analysis of the SiCN powder is given in Table 1. The SiCN powder consisted in particles of irregular shape associated in hard aggregates, that prevented from a precise assessment of the individual particle size. Each particle contained several crystals of β-SiC embedded in a $SiO_xC_yN_z$ amorphous phase. In addition, the silicon in excess appeared in the form of smaller particles (10–30 nm) with rounded shape.[6] The surface area of the SiCN powder was 48 m^2 g^{-1}. The wt% in the green compact were 68·8 Si_3N_4, 22·2 SiCN, 6 Y_2O_3 and 3 Al_2O_3. The 22·2 wt% SiCN led theoretically to 10 wt% SiC.[7] Near full density ($\approx$98·8%) was achieved by increasing the hot-pressing temperature to 1600°C.

The ratio between the α and β polymorphs of Si_3N_4 was obtained following the method used by Rossignot *et al.*[3] which was derived from the procedure developed by Gazzara and Messier.[8] Microstructures were examined in a plane perpendicular to the pressing direction by scanning electron microscopy (SEM, JEOL JSM 35) after plasma-etching and by transmission electron microscopy (TEM, JEOL 2010). The surfaces were coated by carbon then gold to avoid charge effects during the observations.

The microstructure of Si_3N_4 monolith consisted in equiaxed grains of α-Si_3N_4 and slightly elongated grains of β-Si_3N_4 (in fact, the β-$Si_{6-x}Al_xO_xN_{8-x}$ solid solution, but with a very low x due to the low alumina addition) embedded in an intergranular YSiAlON glassy phase (Fig. 1). The low sintering temperature limited grain growth and the mean grain size was $\sim$ 250 to 300 nm. Yttrium was entirely concentrated in the intergranular amorphous phase that, due to the high atomic number of yttrium, was highly electron absorbing and, hence, was always visible in darker contrast than the Si_3N_4 grains. The amorphous phase formed continuous intergranular films and pockets at triple grain junctions, The α/β ratio was 70/30.

In the case of the composite, the α/β ratio was 30/70. The SiC nanoparticles have sizes ranging from 30 to 60 nm. The α-Si_3N_4 grains were equiaxed, but the β-Si_3N_4 grains were mostly equiaxed too, or at least presented a low aspect ratio, even if some of them had a more well-developed acicular morphology [Fig. 2(a)]. The mean grain size was 360 nm. It seems that the SiC nanoprecipitates, though increasing the α to β-Si_3N_4 transformation rate, limit the acicular growth of the β-Si_3N_4 grains.[7] The precipitates were sometimes observed inside the Si_3N_4 grains. However, they were mainly located either along Si_3N_4 grain boundaries or, more often, they were gathered together into pockets, the size of which was similar to that of the individual Si_3N_4 grains. The SiC nanoparticles were well wetted by the amorphous phase so that a great fraction of the glass phase was localised in between the particles [Fig. 2(b)]. As a consequence of this inhomogeneous distribution of the nanoparticles, numerous Si_3N_4–Si_3N_4 grain

Table 1. Elemental analysis and theoretical composition of the SiCN powder

Element analysis (wt%)				*Theoretical composition (wt%)*				*Atomic ratio*
Si	N	C	O	Si_3N_4	SiO_2	SiC	Si	C/N
66·9	18·2	13·6	2·3	45·1	4·3	45·1	5·5	0·87

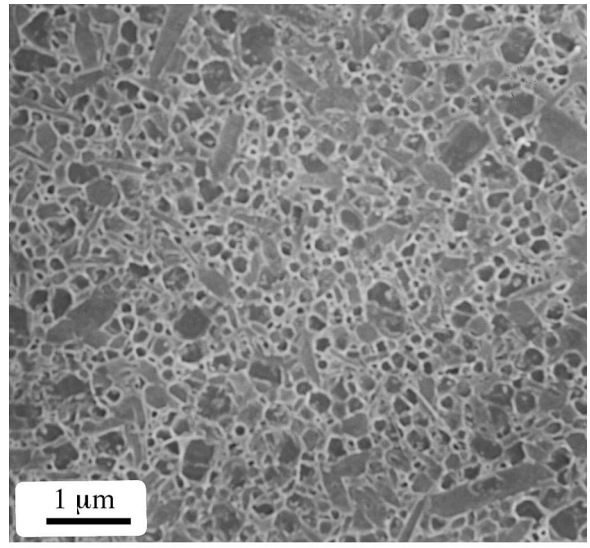

(a)

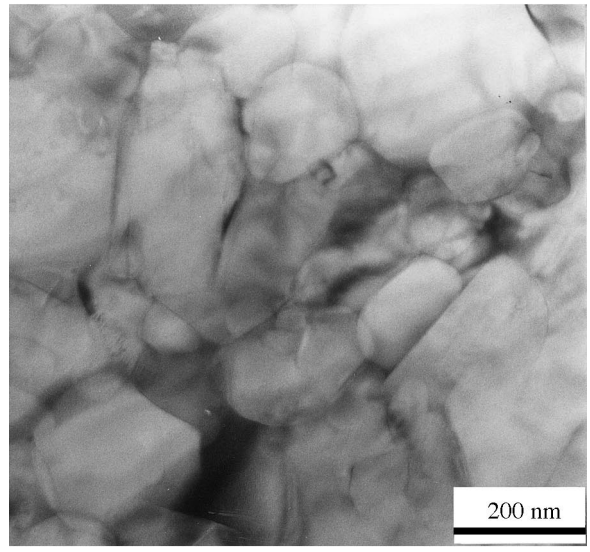

(b)

Fig. 1. Micrographs of the monolith: (a) SEM; (b) TEM.

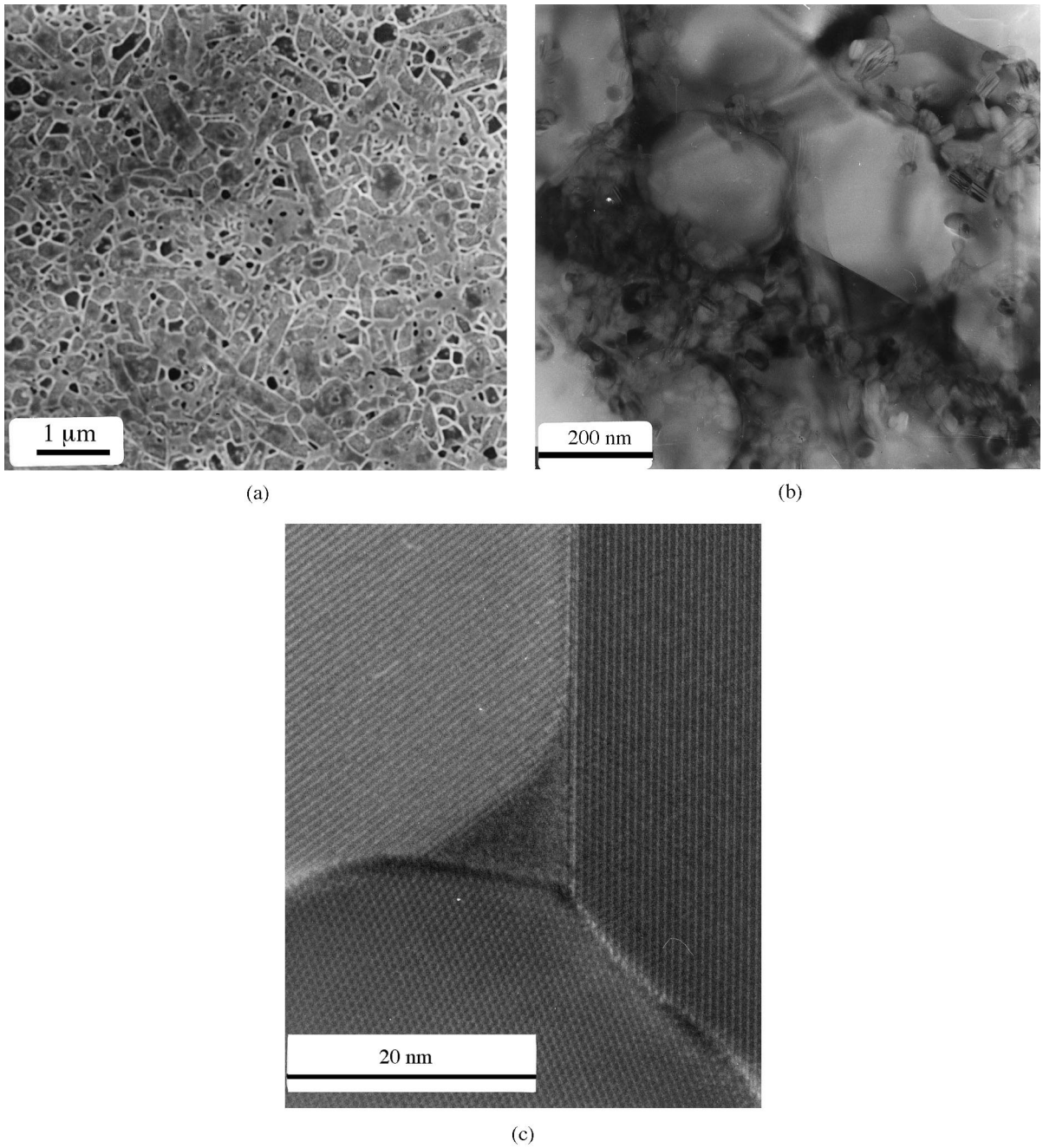

Fig. 2. Micrographs of the composite: (a) SEM; (b) TEM general view; (c) a glass pocket and grain boundaries free of SiC nanoprecipitates.

boundaries were free of SiC nanoparticles, and in this case, the intergranular glass films were very narrow ($\approx$ 1·3 nm) [Fig. 2(c)]. No other crystalline phases were detected either in the monolith or the composite.

The glass transition temperature of the intergranular glass phase can be evaluated through the change in slope when measuring the evolution of Young's modulus with temperature.[9] The results in Fig. 3 show a T_g at about 1050°C for the monolith, consistent with previous studies on such glasses[10,11] and a T_g higher by about 75°C for the composite. The higher viscosity at a given temperature in the composite is likely to be associated with the presence of carbon coming from the SiCN powder.

2.2 Testing

Compressive creep tests were conducted in air environment using a dead load machine. The change in specimen length was monitored with a linear variable differential transformer (LVDT) and a chart recorder, The scatter of the measurement for the deformation was within 2 μm.

The specimens were parallelepipedic bars $3\times3\times8$ mm^3. They were placed between two silicon carbide platens. The parts in contact with the specimen were coated with boron nitride to reduce

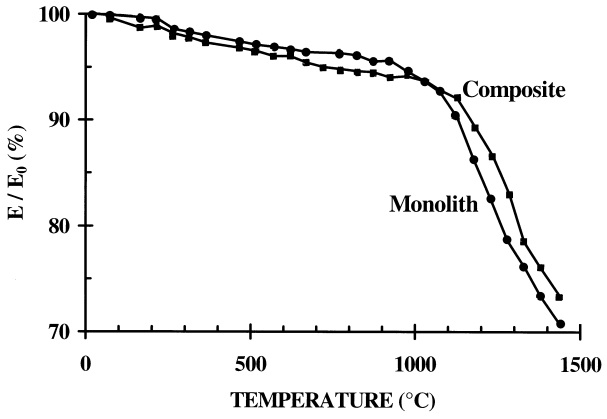

Fig. 3. Change in Young's modulus versus temperature.

friction between the sample and the fixtures. Under these operating conditions, very little barrelling of the samples was observed after testing. The furnace was allowed to stabilise for 45 min at the test temperature before applying the load.

As the tests were conducted under constant load instead of constant stress, as soon as deformation becomes noticeable, true strain (ε_t), true stress (σ_t) and true strain rate ($\dot{\varepsilon}_t$) were calculated from the engineering strain ($\varepsilon_e = [h - h_0]/h_0$), engineering stress ($\sigma_e$) and engineering rate ($\dot{\varepsilon}_e$), using the boundary condition of a constant volume during the deformation. For the frictionless case,[12] the following expressions were used:

$$\varepsilon_t = \ln(1 + \varepsilon_e) \tag{1}$$

$$\sigma_t = (1 + \varepsilon_e)\sigma_e \tag{2}$$

$$\dot{\varepsilon}_t = \dot{\varepsilon}_e[1/(1 + \varepsilon_e)] \tag{3}$$

Though, in compression, ε_t, σ_t and $\dot{\varepsilon}_t$ are negative, their absolute values were considered in drawing the curves.

3 Experimental results

3.1 Creep data

The tests were conducted at constant temperature between 1200 and 1450°C with applied stresses ranging from 45 to 180 MPa. True strain (%) against time data (up to 50 h) are shown in Figs 4 and 5 for the monolith and the composite, respectively. The tests were duplicated at 1250, 1300 and 1350°C. The difference between the corresponding curves was more pronounced for the composite than for the monolith and increased slightly with the temperature. It reached, at worst, about 20%.

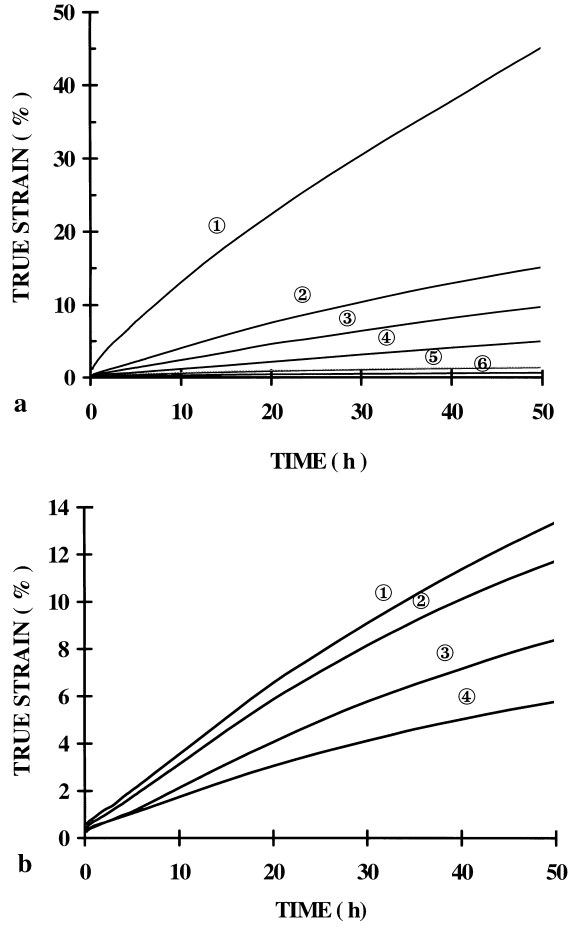

Fig. 4. Creep curves of the monolith: (a) at various temperatures under a nominal stress of 180 MPa, ① 1400, ② 1350, ③ 1330, ④ 1300, ⑤ 1250, ⑥ 1200°C; (b) at 1350°C under various nominal stresses, ① 180, ② 135, ③ 90, ④ 45 MPa.

All the materials exhibit a transient creep followed by a pseudo-stationary creep for the monolith and a quasi-stationary creep for the composite. No tertiary region was observed within the 50 h of duration of the tests. The creep resistances are compared in Fig. 6 under the same test conditions (1350°C, 180 MPa). The creep strain of the monolith is 2·5 times greater than that of the composite. The comparison of the strains at the end of the tests shows that the creep resistance of the composite is similar to that of the monolith at a temperature 50°C higher. The creep data at the end of the 50 h tests are shown in Tables 2 and 3.

Typical true strain rate versus time curves are shown in Fig. 7 for the two materials. For the composite [Fig. 7(b)] the strain rate decreases rapidly during the first 15 h (primary creep) and then slowly to tend toward a nearly constant value. After 35 h, the residual decrease is essentially due to the slow decrease of the true stress (secondary creep). In the case of the monolith, the evolution is similar for temperature $\leq$ 1250°C, but, for higher temperatures [Fig. 7(a)], after the sharp initial decrease, the creep rate goes through a

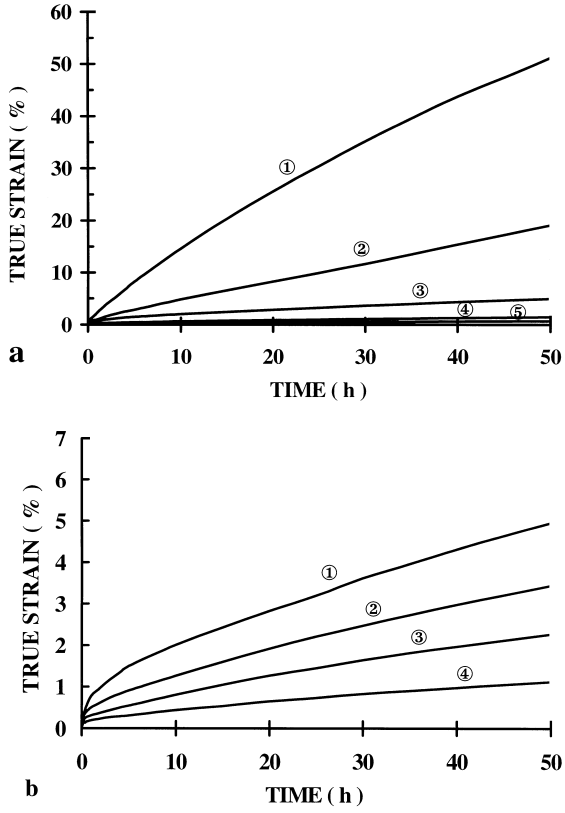

Fig. 5. Creep curves of the composite: (a) at various temperatures under a nominal stress of 180 MPa, ①1450, ②1400, ③1350, ④1300, ⑤1250°C; (b) at 1350°C under various nominal stresses, ①180, ②135, ③90, ④45 MPa.

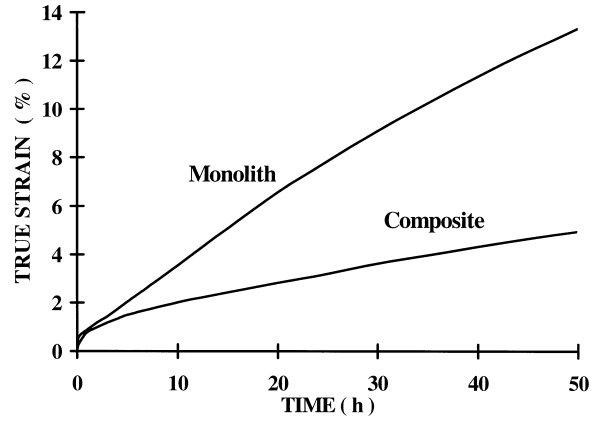

Fig. 6. Comparison of the creep curves of the monolith and the composite under the same condition (1350°C, 180 MPa).

maximum around the 10 h and, next, diminishes slowly (pseudo-stationary creep). In these latter cases, the decrease remains too pronounced to be solely attributed to the decrease of the true stress.

3.2 Stress and temperature dependencies of creep rate.

Creep rate at the end of the tests was related to stress and temperature using the Dorn–Boltzmann relation:

$$\dot{\varepsilon} = Ad^{-p}\sigma^{n}\exp(-E_a/RT)) \qquad (4)$$

where, A is constant, d the mean grain size, p the grain size exponent, σ the stress, n the stress exponent, E_a the apparent activation energy, R the gas constant and T the absolute temperature.

Preliminary stress jump tests on Si_3N_4 monolith showed that a true stationary regime was not obtained even after 100 h. So, to minimise the influence of microstructural changes, the stress exponents were derived from independent isothermal creep curves at 1350°C. The true creep rates were measured after 50 h for nominal stresses of 45, 90, 135, and 180 MPa. Actual stresses, calculated according to eqn (2), were used in the ln $\dot{\varepsilon}$ versus ln σ diagram (see Tables 2 and 3). The values of the stress exponent obtained from the best-fit straight lines were $n = 1{\cdot}05$ for the composite and $n = 0{\cdot}78$ for the monolith (Fig. 8) with correlation factors of 0·997 and 0·983, respectively.

The apparent activation energies were determined using independent creep curves obtained at different temperatures with the same nominal stress. Owing to the change in stress during the tests, the creep rates after 50 h were normalised to 180 MPa by using the stress exponents previously determined. The corrected creep rates could be fitted by an unique straight line in the ln $\dot{\varepsilon}_{corr}$ versus $1/T$ diagram. The apparent activation energies were found to be 590 and 514 kJ mol^{-1} for the composite and the monolith respectively with correlation factors of 0·973 and 0·957 (Fig. 9).

3.3 Microstructure and phase changes

After creep testing in air for 50 h, the samples of Si_3N_4 monolith were covered with a scale, white in colour, and showed underneath a zone depleted in yttrium (Fig. 10). The thickness of the scale increased with temperature. At 1350°C, the width of the oxide scale was about 100 μm and the depth of the depleted zone about 400 μm. In contrast, the surface of the composite samples was black and the zone depleted in yttrium only about 100 μm. For comparison, in a sample of Si_3N_4 monolith oxidised without load under the same conditions, the thickness of the oxide scale was only about 10 μm, XRD results and SEM observations showed the scale consisted in an amorphous glaze into which were embedded crystals of cristobalite and yttrium disilicate [Fig. 10(c)]. At the highest temperature used (1450°C), crystals were rare and the oxidation scale consisted mainly in an amorphous phase punctured by numerous pores. This behaviour is classically observed for similar silicon nitride ceramics.[13–15] It results from outward diffusion of yttrium from the intergranular phase in the high silica glass produced by oxidation of the Si_3N_4 grains to established chemical equilibrium between

Table 2. Creep data for the monolith at the end of a 50 h test

	T (°C)								
	1200	*1250*	*1300*	*1330*	*1350*				*1400*
σ_t(MPa)	178·9	177·4 177·5	171·3 170·8	163·3	42·47	82·76	120·07	157·5 154·3	114·6
$\varepsilon_t(10^{-2})$	0·61	1·45 1·38	4·95 5·22	9·73	5·77	8·38	11·72	13·3 15·1	45·1
$\dot{\varepsilon}_l(10^{-8}s^{-1})$	1·98	3·15 3·55	25·5 22·9	43·5	19·52	32·77	42·05	51 58	209
$\dot{\varepsilon}_{t\ corr.}$ $(10^{-8}\ s^{-1})$	1·99	3·18 3·58	26·5 23·9	46·9				56·5 65·7	297

Table 3. Creep data for the composite at the end of a 50 h test

	T (°C)							
	1250	*1300*	*1350*				*1400*	*1450*
σ_t(MPa)	178·75 178·75	177·4 176·5	44·5	88	130·40	171·3 168·9	147	108
$\varepsilon_t(10^{-2})$	0·7 0·71	1·45 1·98	1·1	2·27	3·44	4·95 6·34	20	51·1
$\dot{\varepsilon}_t$ $(10^{-8}\ s^{-1})$	2·22 2·22	5·3 6·7	4·2	8·44	12·10	17·6 23·7	134	211·8
$\dot{\varepsilon}_{t\ corr.}$ $(10^{-8}\ s^{-1})$	2·22 2·22	5·4 6·8				18·5 25·3	164·1	353

the oxidised scale and the inner material. The precipitation of silica and yttrium disilicate occurs because the equilibrium conditions change with time as oxidation proceeds.[15] At the highest temperature, the viscosity of the glass is low enough to allow molecular nitrogen bubbles, formed at the internal interface, to migrate through the fluid scale, creating an interconnected porosity.[13]

The α/β-Si_3N_4 ratio in the composite samples remained unchanged during creep tests up to 1350°C, diminished slightly at 1400°C and the α-phase was no longer detected after creep at 1450°C (Table 4). For the monolith, the α/β ratio decreased slowly up to 1300°C and then rapidly for higher temperatures. In both cases, once the oxidised scale had been removed, no other crystalline phases were detected by RD in addition to SiC and the Si_3N_4 polymorphs.

No signs of cavitation were evidenced in both materials by TEM investigation, that is consistent with the absence of a tertiary regime on the creep curves. The most distinctive deformation induced features were strain whorls located in grain

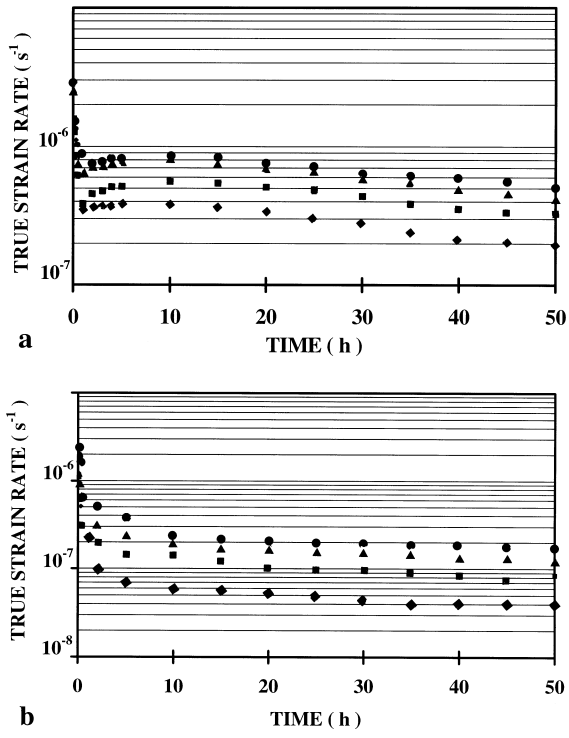

Fig. 7. True strain rates versus time at 1350°C under various nominal stresses, ● 180, ▲ 135, ■ 90, ◆ 45 MPa: (a) monolith; (b) composite.

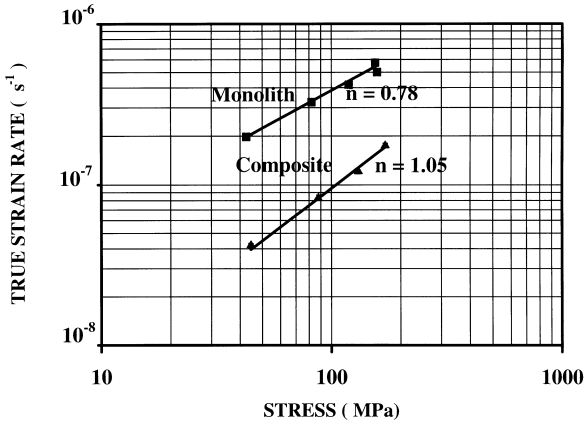

Fig. 8. True strain rate versus true stress.

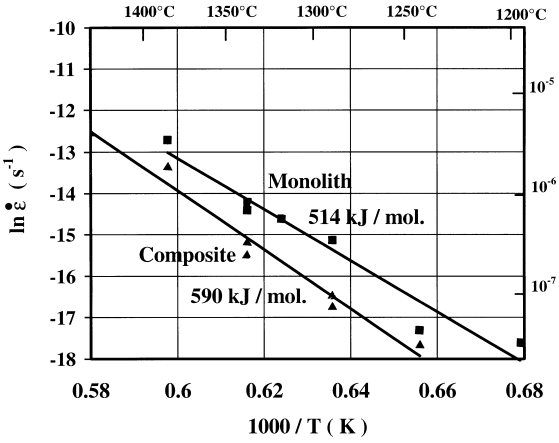

Fig. 9. True strain rate versus reciprocal absolute temperature.

boundaries with thin glassy film (Fig. 11), and, in the case of the monolith, an increased number of acicular grains.

4 Discussion

4.1 Creep mechanisms

It is well established that creep of ceramics containing a noticeable amount of intergranular amorphous phase (~10%) is primarily controlled by this intergranular phase.[16] This is illustrated by the absence of significant dislocation activity inside the crystals and by the fact that creep deformation becomes measurable above the glass transition temperature of the intergranular phase (T_g~1050°C in the present case). Typically, the creep curves exhibit a primary stage followed by a long pseudo-stationary stage.

Though cavity formation is more difficult under compressive applied stresses than under tensile ones, cavitation can occur, particularly at high stresses. Then, a tertiary stage is generally observed. Failure occurs when a crack of critical size is formed by the linkage of microcracks resulting from the growth and coalescence of the cavities increasing in size and number. In a hot-pressed silicon nitride densified with 8 wt% Y_2O_3 and 3 wt% Al_2O_3, Crampon *et al.*[17] found that cavitation participates in substantial deformation in compressive tests continued up to failure in the 1270–1330°C temperature range but with stresses ranging from 175 to 300 MPa. A comparison could be done between their 1300°C–175 MPa test (Fig. 1 in Ref.[17]) and the 1300°C–180 MPa test of the present work [Fig. 4(a)]. The creep deformation is smaller in our case, due to the smaller amount of Y_2O_3 additive, resulting in a smaller amount of amorphous phase. In their test, a tertiary creep, dominated by cavitation, started after 60 h; so, the reason why tertiary was not observed during our experiments, even under the highest stress used, may be because tests were stopped after a 50 h duration, that is before cavitation develops. Yoon

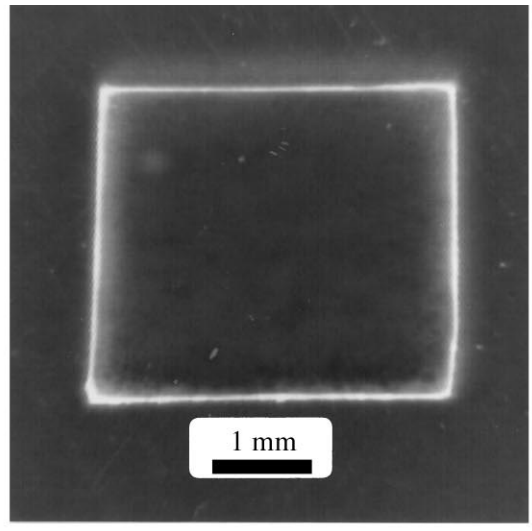

(a)

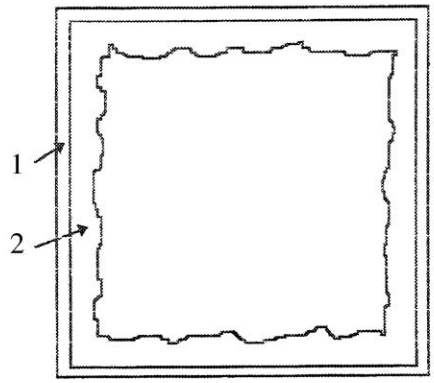

(b)

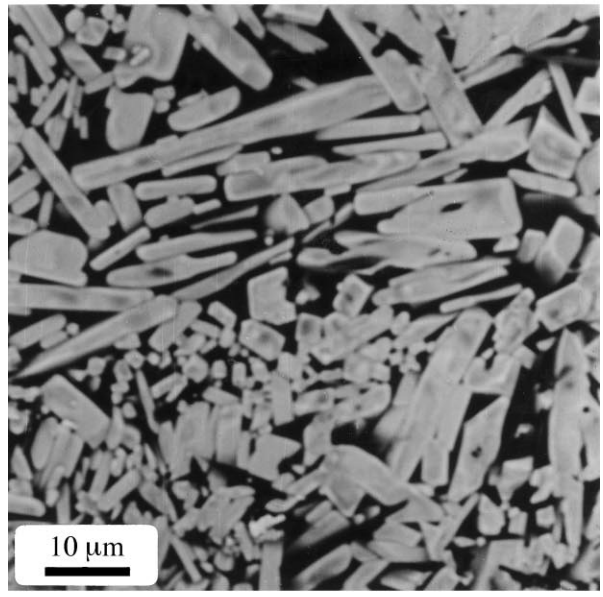

(c)

Fig. 10. Si_3N_4 monolith crept 50 h at 1350°C under 180 MPa: (a) optical macrograph of a cross section; (b) schematic drawing (1) oxide scale, (2) zone depleted in yttrium; (c) SEM micrograph of the oxide scale of a sample crept at 1350°C.

Table 4. α/β-Si_3N_4 ratio after creep tests

	Temperature (°C)						
	25	*1200*	*1250*	*1300*	*1350*	*1400*	*1450*
Monolith	70/30	68/32	66/34	60/40	48/52	29/71	
Composite	32/68		31/69	30/70	31/69	25/75	0/100

et al.[18] have studied silicon nitride ceramics (labelled SN11 and SN15) which resemble the present monolith: same grade of Si_3N_4 powder, same additives but with a smaller content in Y_2O_3. As in our case, and in similar temperature (1300–1400°C) and stress (30–100 MPa) ranges, they did not observe either cavitation or crystallisation of the amorphous phase during tests. The better creep resistance obtained by Yoon *et al.*[18] is to be linked to the smaller amount of additives and to the acicular morphology of the Si_3N_4 grains in their materials. Creep mechanisms involving cavitation, usually associated with values of stress exponent >2, require much higher stress levels than used in this study and must be ruled out to explain our results.

In silicon nitride ceramics with similar amounts of glass phase, it has been shown that the primary stage is dominated by the viscoelastic response of the glass phase itself.[16,19] Arons and Tien[19] proposed that, under the applied stress, large pressure gradients appear, making the glass phase flow from high pressure regions to lower pressure regions. The redistribution of the glass phase is supported by the observation of Jin *et al.*[20] that the standard deviation of the film thickness is considerably larger after creep than before. A macroscopic gradient appears also between the bulk and the surface so that a noticeable fraction of the glass phase is exuded to the surface during the very first hours of the test.[21,22] The depth of the zone affected by this mechanism is about 1·5 mm.[23] The contribution due to the viscoelastic response of the glass phase vanishes in about 20 h. This exudation results in an improved packing of the grains with a marked decrease of the size of the glass pockets at triple grain junctions and of the width of the intergranular films.[22] Then, grain boundary sliding becomes restricted by grain-to-grain contacts at asperities. These contacts give rise to an elastic deformation of the regions adjacent to the buttressing points that is evidenced by localised 'strain whorls' observed in crept samples cooled under load. The building up of the resulting stress fields, as the width of the intergranular films becomes thinner, results in a strain hardening effect, i.e. an ever decreasing creep rate, which explains the long pseudo-stationary stage. Meanwhile, differential chemical potentials that arise due to stress gradients provide the driving force for a solution–migration–precipitation process resulting in a diffusional creep.[16] A true stationary creep is reached when the recovery effect due to diffusional creep compensates the strain hardening effect.

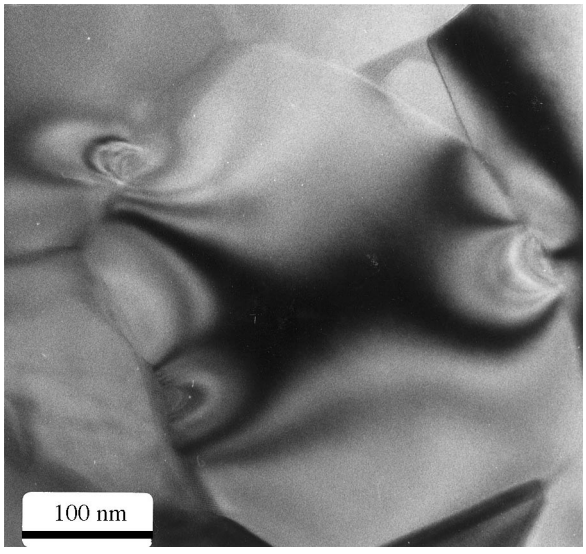

Fig. 11. TEM micrograph of a monolith sample crept at 1350°C showing strain whorls along grain boundaries.

This scenario applies to the composite. The microstructure is stable: the transformation of the α-Si_3N_4 phase does not occur at temperatures $<$ 1400°C and the nanosized SiC grains located along the grain boundaries inhibit grain growth. A true stationary stage is reached in about 30 h.

In the case of the monolith, the situation is complicated by the evolution of the α/β-Si_3N_4 ratio during the test at temperatures $\geq$ 1300°C. This Si_3N_4 material was densified at a temperature low enough to result in a microstructure consisting in fine, equiaxed grains of the α-polymorph as the major crystalline phase ($\alpha/\beta = 70/30$). This microstructure was tailored to allow superplastic forming.[3,24] The α to β transformation, slow for $\alpha/\beta > 50/50$, becomes rapid for $\alpha/\beta < 50/50$. The time needed to reach the transition between the two regimes is 10 h at 1500°C. It increases when the temperature decreases, but this time is reduced under stress.[25] As it is not observed in the composite, where the β/α ratio remains constant up to 1400°C, the maximum in the creep rate around the

10th hour is very likely to be associated with this transformation. The transformation is accompanied by an increase in the quantity of liquid phase and the precipitation of small sized β-Si_3N_4 grains, that favours an increase of the creep rate. Later, the strain hardening due to the acicular growth of the β-Si_3N_4 grains has the upper hand and the creep rate decreases. Eventually, grain-to-grain contacts form and the behaviour is then similar to the one observed in low α-Si_3N_4 containing silicon nitride ceramics.

As reported in Section 3·3, the oxidised scale of the monolith is 10 times thicker under stress. In this temperature range, the oxidation of the Si_3N_4 grains is very slow whereas the oxidation of oxynitride glasses belonging to the Y–Si–Al–O–N system is complete within a few hours above 1100°C and is accompanied by a strong volume expansion.[26] The slow oxidation of the Si_3N_4 grains is illustrated by the low thickness (10 μm) of the oxide scale on the monolith exposed in air without an applied stress. At the same temperature, the dramatically thicker oxide scale on the crept monolithic samples results from the oxidation of the glass exuded on the surface of the samples during the first hours of the tests. This was confirmed by the fact that the white oxide scale was in excess to the dimensional changes due to creep deformation. In the case of the composites, the thinner oxidation scale results from a less quantity of exuded glass. The reasons for this are the higher viscosity of the glass and its better oxidation resistance due to the presence of carbon (also responsible of the black colour), the fact that the intergranular films are either very thin or obstructed by SiC nanoprecipitates and, as will be discussed in Section 4·4, the trapping of a large amount of glass in the stress-free pockets at triple junctions.

4.2 Stress exponent

Rouxel *et al.*[24] have recently reviewed the values of the stress exponents reported in the literature for both tensile and compressive tests on silicon nitride ceramics. A U-shape domain could be drawn with a minimum (lowest n value) for an applied compressive stress of 80 MPa, that brings out an asymetric behaviour between tension and compression. Furthermore, in a compressive stress range extending from 20 to 200 MPa, shear thickening ($n < 1$) was observed.[18,27–29] To explain the transition from Newtonian behaviour to shear thickening above $\sigma^* = 20$ MPa, Chen and Hwang[27] have extended to silicon nitride a continuous mechanics model initially developed by Yoon and Chen[30] for the superplastic flow of two-phase ceramics containing rigid inclusions in a soft matrix. They consider that, when the normal pressure on a grain boundary exceeds a certain critical stress σ_c, the small region containing this grain boundary becomes rigid and play the role of a rigid inclusion. They identify the volume fraction of the 'rigid phase' with the fraction of grain boundaries that support a normal pressure in excess of σ_c and they envision that this fraction increases with stress above an applied stress $\sigma^* = \frac{2}{3}\sigma_c$ Their model predicts a transition from Newtonian behaviour at stresses $< \sigma^*$ to shear thickening at stresses $> \sigma^* = 20$ MPa. They suggest that the critical stress is the stress needed for the grain boundary liquid be entirely squeezed out except the Stern layers. Chen and Hwang[27] assumptions were recently supported by Burger *et al.*[31] who observed that strain whorls were found preferentially on those grain boundaries that were almost perpendicular to the applied stress. However, strain whorls can also result from the buttressing of adjacent grains at ledges[32] frequently observed along boundaries formed by a low index plane.[33] Moreover, when the stress exponent is measured during a pseudo stationary stage, as is the case here, values less than 1 are obtained, approaching a limiting value $n = 1$ after very long test times.[34,35] Apparent stress exponent $n < 1$ was also observed in polycrystalline yttria[36] as a result of dynamic grain growth.

When a true stationary stage is reached, as is the case for the composite, for which grain growth is inhibited by the SiC particles and no further α to β transformation is observed during test up to 1400°C, the stress exponent is equal to unity, characteristic of a Newtonian diffusional creep. For this reason, we suspect the structural changes resulting from the polymorphic transformation to be responsible for the apparent shear thickening in the monolith.

4.3 Activation energy

The apparent activation energy for the composite was measured in the steady-state creep. As shown above, the contribution to the creep deformation due to flow and redistribution of the viscous phase must be considered as negligible in this stage. A stress exponent of 1 and strain whorls at highly stressed contact points are evidence for grain boundary sliding accommodated by a solution–migration–precipitation mechanism. This mechanism must be controlled by the slowest of the two steps: either by the solution of Si_3N_4 in the glass phase (interface reaction) or by the transport of matter through the glass phase (diffusion). In the interface limited case, the activation energy must be close to the heat of solution of crystalline Si_3N_4 in the glass which has been estimated[37] to be roughly 400 kJ mol^{-1}. The diffusivity in the glass phase can be related to the viscosity of the glass

through the Stokes–Einstein equation, so that the activation energy in the diffusion limited case is the same as that for viscosity.[38] The activation energy for the viscosity of Y–Si–Al–O–N glasses were measured by Rouxel *et al.*[39] to be about 1000 kJ mol^{-1} at 900°C and to decrease slowly as the temperature increases. This value of the activation energy for viscous flow of oxynitride glasses was recently confirmed[40] from the study of the shear viscosity of a Y–Mg–Si–Al–O–N glass join between two Si_3N_4 parts for which a value of 950 kJ mol^{-1} was measured between 880 and 970°C.

Activation energies reported in the literature (Table 5) range from 720 up to 1260 kJ mol^{-1} for silicon nitride ceramics densified with Y_2O_3 alone[41–44] and from 640 to 800 kJ mol^{-1} when Y_2O_3 and Al_2O_3 are used together.[17,30,38,45,46] Two exceptions are a grade studied by Yoon *et al.*[30] (400 kJ mol^{-1}) and the value of 430 kJ mol^{-1} measured by Nixon *et al.*[46] between 1200 and 1300°C. For the material with $E = 400$ kJ mol^{-1}, Yoon *et al.*[30] suggested that the creep deformation was mainly controlled by solution–reprecipitation of Si_3N_4 grains. Ohji *et al.*[45] proposed that, for their materials, the creep was controlled by a steady state mechanism such as creep with a linear increase in the number of facet-sized cavities. For the other materials, the different authors concluded that diffusion through the intergranular glass phase was the rate limiting step, independently of the occurrence of cavitation or not.

For Si_3N_4/SiC nanocomposite materials, crept in 4-point bending, Rendtel *et al.*[43] measured activation energies ranging from 975 to 1085 kJ mol^{-1}, with an activation energy as high as 1435 kJ mol^{-1} for one grade. For Si_3N_4/SiC whisker composites, Ohji *et al.*[45] found 1030 to 1190 kJ mol^{-1} under tensile solicitations, whereas, under compressive stresses ranging from 100 to 300 MPa, Nixon *et al.*[46] observed a change in the activation energy from about 400 kJ mol^{-1} for T between 1200 and 1300°C to about 700 kJ mol^{-1} for T between 1300 and 1400°C. They concluded that in the low temperature regime grain boundary sliding was controlled by diffusion through the glass phase whereas in the high temperature regime, grain boundary sliding was joined by a parallel mechanism of cavitation.

In the present study, the value of the activation energy for the composite ($E = 590$ kJ mol^{-1}) is somewhat lower than the lower limit of activation energies generally associated with diffusion controlled creep. Moreover, it is significantly lower than the values measured by Rendtel *et al.*[43] for Si_3N_4/SiC nanocomposites. On the contrary, it is slightly higher than the value associated by Nixon *et al.*[46] to diffusion controlled creep in Si_3N_4/SiC whisker composites.

Though it seems clear that the creep process involves solution, diffusive transport and reprecipitation steps, the apparent activation energy depends on a number of different factors as noted

Table 5. Activation energy and mechanism for various silicon nitride based ceramics

Authors	*Sintering aids (wt%)*	*Temperature (°C)*	E *(kJ mol^{-1})*	*Solicitation*	*Cavitation*	*Mechanism*
Silicon nitride monoliths						
Ferber *et al.*[40]	$4Y_2O_3$	1260–1370	795/930	Tension	Yes	Diffusion
Menon *et al.*[41]	$4Y_2O_3$	1150–1400	980	Tension	Yes	Diffusion
Wiederhorn *et al.*[43]	$8Y_2O_3$	1400–1500	980	4 pt. bending	Yes	Diffusion
Rendtel *et al.*[42]	$4Y_2O_3$	1330–1430	1260	Tension	Yes	Not specified
Ohji *et al.*[44]	$5Y_2O_3 + 3Al_2O_3$	1200–1350	1065	Tension	Yes	Cavitation
Yoon *et al.*[29]	$9{\cdot}7Y_2O_3 + 7{\cdot}2Al_2O_3$	1300–1400	700	Compression	No	Diffusion
Yoon *et al.*[29]	$4{\cdot}3Y_2O_3 + 3{\cdot}23Al_2O_3$	1300–1400	700	Compression	No	Diffusion
Tood *et al.*[37]	$6Y_2O_3 + 2Al_2O_3$	1300–1400	690	4 pt. bending	Yes	Diffusion
Crampon *et al.*[17]	$8Y_2O_3 + 3Al_2O_3$	1270–1330	650	Compression	Yes	Diffusion
Nixon *et al.*[45]	$6Y_2O_3 + 1{\cdot}5Al_2O_3$	1300–1400	640–800	Compression	Yes	GBS + cavitation
Nixon *et al.*[45]	$6Y_2O_3 + 1{\cdot}5Al_2O_3$	1200–1300	430	Compression	No	Diffusion
Yoon *et al.*[29]	$3{\cdot}3Y_2O_3 + 2{\cdot}5Al_2O_3$	1300–1400	400	Compression	No	Interface
Si_3N_4/SiC nanocomposites						
Rendtel *et al.*[42]	$4Y_2O_3$-SiC B	1400–1500	975	4 pt. bending	Yes	Not specified
Rendtel *et al.*[42]	$4Y_2O_3$-SiC plasma	1400–1500	985	4 pt. bending	Yes	Not specified
Rendtel *et al.*[42]	$4Y_2O_3$-SiC precursor	1400–1500	1050–1435	4 pt. bending	Yes	Not specified
Si_3N_4/SiC whisker-reinforced ceramics						
Ohji *et al.*[44]	$5Y_2O_3 + 3Al_2O_3$	1200–1350	1030–1190	Tension	Yes	Cavitation
Nixon *et al.*[45]	$6Y_2O_3 + 1{\cdot}5Al_2O_3$	1300–1400	500–750	Compression	Yes	Viscous flow
Nixon *et al.*[45]	$6Y_2O_3 + 1{\cdot}5Al_2O_3$	1200–1300	240–360	Compression	No	Diffusion

by Raj and Morgan.[37] the heat of solution of the β-Si_3N_4 crystal in the glass, ΔH_s, the activation enthalpy barrier across the interface, ΔH_1, the enthalpy of the viscosity, ΔH_g, which is itself temperature dependent. ΔH_s and ΔH_1 are only roughly estimated and ΔH_g has only been measured in a temperature range (850–1000°C) significantly lower than the temperature domains usually investigated in creep experiments. The problem is complicated by possible local and/or time-dependent variations of glass composition resulting from surface oxidation and/or partial crystallisation of the glass. In this context, and with a possible additional influence of the SiC nanoparticles in the case of the composite and of the α to β transformation in the monolith, it is difficult to conclude which of the two steps (dissolution or diffusion) is rate controlling.

4.4 Creep resistance

Since the stress exponents and the apparent activation energies of the monolith and of the composite are basically the sames, the difference in creep resistance must derive from differences in microstructure. Several features can be put forward to explain the better resistance of the composite: (i) the intergranular phase in the composite is more refractory than in the monolith as evidenced by the change in Young's moduli with temperature, (ii) the SiC grains present in the intergranular films obstruct the easy paths of diffusion, (iii) due to their larger size, the Si_3N_4 grains form a rigid network that transmit the stresses so that the SiC grains gathered together in pockets are virtually stress-free and do not contribute to the deformation, (iv) because of the trapping of a large amount of glass phase in these stress-free SiC grain pockets, the intergranular films in the composite are thinner than in the monolith.

5 Conclusion

The creep behaviour of Si_3N_4/SiCN composite and of the corresponding matrix is governed by grain boundary sliding accommodated by diffusion through the intergranular glass phase.

The SiCN nanoparticles lead to the formation, during sintering of SiC nanoprecipitates, mainly situated in the intergranular phase, either along grain boundaries or gathered in pockets, and to the incorporation of some carbon in the glass phase, that increases its viscosity.

In the temperature range 1250–1400°C, the microstructure of the composite remains unchanged whereas the α to β-Si_3N_4 ratio increases in the monolith.

The better creep resistance of the nanocomposite is explained by:

1. a more refractory intergranular glass phase due to the presence of carbon,
2. the presence of SiC nanoprecipitates that obstruct the easy paths of diffusion that are the intergranular glass films which are also thinner than in the monolith due to the trapping of a large amount of glass in the SiC pockets,
3. the fact that the SiC nanoparticles gathered in the pockets are virtually stress-free and do not participate to the deformation.

Acknowledgements

This work was supported by the CNRS in the frame of the GDR 1168 'Poudres céramiques monophasiques à base de silicium'. The authors are grateful to all the participants in the GDR for fruitful collaboration. We wish to thank Dr J. P. Erauw of VITO (Mol, Belgium) for the plasma etching. Details on the structure and texture of the starting SiC-based nanopowders were provided by M. Monthioux and C. Béraud, CERES, UPRA-8011 CNRS, 31055 Toulouse, France.

References

1. Wakai, F., Kodama, Y., Sakaguchi, S., Murayama, N., Izaki, K. and Niihara, K., A superplastic covalent crystal composite. *Nature*, 1990, **344**, 421–423.
2. Rouxel, T., Wakai, F. and Izaki, K., Tensile ductility of superplastic Al_2O_3–Y_2O_3–Si_3N_4/SiC composites. *J. Am. Ceram. Soc.*, 1992, **75**, 2363–2372.
3. Rossignol, F., Rouxel, T., Besson, J-L., Goursat, P. and Lespade, P., Superplasticity in silicon nitride through the α to β phase transformation. *J. Phys. III France*, 1995, **5**, 127–134.
4. Madigou, V., Monthioux, M. and Oberlin, A. Microstructure et microtexture d'un composite Si_3N_4 renforcé whiskers SiC et de ses constituents. In *Actes du Colloque ''Matériaux composites pour applications à hautes températures'*, ed. R. Naslain, J. Lamalle and J-L. Zulian. AMAC, Paris, 1990, pp. 221–235.
5. Luce, M., Croix, O., Robert, C. and Cauchetier, M., Laser synthesis of ultrafine Si/C/N composite powders. In *Ceramic Powder Sc., III*, Ceramic Trans. Vol. 12, ed. G. L. Messing, S. I. Hihane and H. Hausner, The American Ceramic Soc. Westerville, OH, 1990, pp. 267–274.
6. Monthioux, M. and Béraud, C., private communication; details can be found in Mayne, M., Elaboration, microstructure et comportement au fluage de nanocomposites Si_3N_4/SiC Doctorate thesis, Université, de Limoges, France, 1997.
7. Mayne, M., Babloul-Hourlier, D. and Goursat, P., Si_3N_4/SiC(N) nanocomposites: influence of SIC(N) nanoprecipitates on the microstructure. In *Euro-Ceramics V*, Vol. 132–136, Part 2. ed. P. Abelard, A. Autissier, A. Bouquillon, J-M. Haussonne, A. Mocellin B. Raveau and F. Thevenot. Trans. Tech. Publications, Vetikon-Zurich, Switzerland, 1997, pp. 998–1001.

8. Gazzara, C. P. and Messier, D. R., Determination of phase content of Si_3N_4 by X-ray diffraction analysis. *Am. Ceram. Bull.*, 1977, **56**, 777–780.
9. Rouxel, T., Besson, J-L., Gault, C., Goursat, P., Leigh, M. and Hampshire, S., Viscosity and Young's modulus of an oxynitride glass. *J. Mater. Sci. Lett.*, 1989, **8**, 1158–1160.
10. Hampshire, S., Drew, R. A. L. and Jack, K. H., Oxynitride glasses. *Phys. Chem. Glasses*, 1985, **26**, 182–186.
11. Lemercier, H., Rouxel, T., Fargeot, D., Besson, J-L. and Piriou, B., Yttrium SiAlON glasses: structure and mechanical properties — elasticity and viscosity. *J. Non-Cryst. Solids*, 1996, **201**, 128–145.
12. Debschütz, K. D., Caspers, B., Schneider, G. A. and Petzow, G., Critical evaluation of the compressive creep test. *J. Am. Ceram. Soc.*, 1993, **76**, 2468–2474.
13. Goursat, P. and Besson, J-L., Corrosion and mechanical properties of silicon nitride based ceramics. Influence of microstructural changes. In *The Physics and Chemistry of Carbides, Nitrides and Borides*. ed. R. Freer. Kluwer Academic, Dordrecht, The Netherlands, 1990, pp. 405–421.
14. Chartier, T., Besson, J-L. and Goursat, P., Microstructure, oxidation and creep behaviour of a β'-Sialon ceramic. *Int. J. High Tech. Ceram.*, 1986, **2**, 33–45.
15. Babini, G. N., Bellosi, A. and Vincenzini, P., Factors influencing structural evolution in the oxide of hot-pressed Si_3N_4–Y_2O_3–SiO_2 materials. *J. Mater. Sci.*, 1984, **19**, 3487–3497.
16. Lange, F. F., Davis, B. I. and Clarke, D. R., Compressive Creep of Si_3N_4/MgO alloys. Part 1, Effect of composition. *J. Mater. Sci.*, 1980, **15**, 601–610.
17. Crampon, J., Duclos, R., Peni, F., Guicciardi, S. and De Portu, G., Compressive creep and creep failure of $8Y_2O_3$/$3Al_2O_3$ doped hot-pressed silicon nitride. *J. Am. Ceram. Soc.*, 1997, **80**, 85–91.
18. Yoon, S. Y., Akatsu, T. and Yasuda, E., The microstructure and creep deformation of hot-pressed Si_3N_4 with different amounts of sintering additives. *J. Mater. Res.*, 1996, **11**, 120–126.
19. Arons, R. M. and Tien, J. K., Creep and strain recovery in hot-pressed silicon nitride. *J. Mater. Sci.*, 1980, **15**, 2046–2058.
20. Jin, Q., Ning, X. G., Wilkinson, D. S. and Weatherly, G. C., Redistribution of a grain phase during creep of silicon nitride ceramics. *J. Am. Ceram. Soc.*, 1997, **80**, 685–691.
21. Clarke, D. R., High temperature deformation of a polycrystalline alumina containing a glass phase. *J. Mater. Sci.*, 1985, **20**, 1321–1332.
22. Besson, J-L., Streicher, E., Chartier, T. and Goursat, P., Viscoelastic creep of nitrogen ceramics. *J. Mater. Sci. Lett.*, 1986, **5**, 803–805.
23. Rouxel, T., Besson, J-L. and Goursat, P., Improvement of creep resistance of sintered silicon nitride by hot isostatic exudation of intergranular glass. *J. Am. Ceram. Soc.*, 1993, **76**, 2790–2794.
24. Rouxel, T., Rossignol, F., Besson, J-L. and Goursat, P., Superplastic forming of an α-phase rich silicon nitride.. *J. Mater. Res.*, 1997, **12**, 480–492.
25. Rossignol, F., Niture de silicium monolithique et composites à fibres courtes Si_3N_{4m}/SiC_f: relations microstructure — renforcement — déformation plastique à haute température. Doctorate thesis, University of Limoges, France, 1995.
26. Sebaï, M., Sjöberg, J., Goursat, P, Nestor, E., Flynn, R., Ramesh, R. and Hampshire, S., Oxidation behaviour of yttrium and neodymium oxynitride glasses. *Journal of the European Ceramic Society*, 1995, **15**, 1015–1024.
27. Chen, I. W. and Hwang, S. L., Shear thickening creep in superplastic silicon nitride. *J. Am. Ceram. Soc.*, 1992, **75**, 1073–1079.
28. Crampon, J., Duclos, R. and Rakotoharisoa, N., Creep behaviour of $Si_3N_4/Y_2O_3/Al_2O_3$/AIN alloys. *J. Mater. Sci. Lett.*, 1993, **28**, 909–916.
29. Burger, P., Plasticité à haute température et microstructure de déformation de nitrure de silicium densifié par compression isostatique à chaud avcc Y_2O_3 et Al_2O_3. Doctorate thesis, University of Lille, France, 1994.
30. Yoon, C. K. and Chen, I. W., Superplastic flow of two-phase ceramics containing rigid inclusions-zirconia/mullite composites. *J. Am. Ceram. Soc.*, 1990, **73**, 1555–1565.
31. Burger, P, Duclos, R. and Crampon, J., Microstructure characterization in superplastically deformed silicon nitride. *J. Am. Ceram. Soc.*, 1997, **80**, 879–885.
32. Lange, F. F., Clarke, D. R. and Davis, B. I., Compressive creep Of Si_3N_4/MgO alloys. Part 2, Source of viscoelastic effect.. *J. Mater. Sci.*, 1980, **15**, 611–615.
33. Clarke, D. R. and Thomas, G., Grain boundary phase in a hot-pressed MgO fluxed silicon nitride. *J. Am. Ceram. Soc.*, 1977, **60**, 611–615.
34. Karunaratne, B. S. B. and Lewis, M. H., Grain-boundary de-segregation and intergranular cohesion in Si–Al–O–N ceramics. *J. Mater. Sci.*, 1980, **15**, 1781–1789.
35. Besson, J-L., Bouarroudj, A. and Goursat, P., Résistance au fluage à l'air d'une céramique de type SiYON frittée sous charge. *Rev. Int. hautes Tempér. Réfract. Fr.*, 1982, **19**, 381–392.
36. Besson, J-L., Murat, D., Rouxel, T., Valin, F., Schnedecker, G. and Boncoeur, M., High temperature mechanical behaviour of polycrystalline yttria. In *Fourth Euro Ceramics. Basic Science — Optimisation of Properties and Performance by Improved Design and Microstructural Control*, Vol. 3, ed. S. Meriiani and V. Sergo. Gruppo Editoriale Faenza Editrice S.p.A. Faenza, Italy, 1995, pp. 147–154.
37. Raj, R. and Morgan, P. E. D., Activation energies for densification, creep, and grain-boundary sliding in nitrogen ceramics. *Com. Am. Ceram. Soc.*, 1981, **64**, C143.
38. Todd, J. A. and Xu, Zhi-Yue, The high temperature creep deformation of Si_3N_4–$6Y_2O_3$-$2Al_2O_3$. *J. Mater. Sci.*, 1989, **24**, 4443–4452.
39. Rouxel, T., Huger, M. and Besson, J-L., Rheological properties of Y–Si–Al–O–N glasses: elastic moduli, viscosity and creep. *J. Mater. Sci.*, 1992, **27**, 279–284.
40. Rouxel, T., Pradeau, D., Besson, J-L., Verdier, P. and Baron, B., Shear viscosity of an oxynitride glass interlayer. In *Euro-Ceramics V*, Vol. 132–136, Part 1, ed. D. Bortzmeyer, M. Boussuge Th. Chartier, G- Fantozzi, G. Lozes and A. Rousset, Trans. Tech. Publications, Vetikon-Zurich, Switzerland, 1997, pp. 563–566.
41. Ferber, M. K., Jenkings, M. G., Nolan, T. A. and Yeckley, R. L., Comparison of the creep and creep rupture performance of two HIPed silicon nitride ceramics. *J. Am. Ceram. Soc.*, 1994, **77**, 657–665..
42. Menon, M. N., Fang, Ho T., Wu, D. C., Jenkings, M. G., Ferber, M. K., More, K. L., Hubbard, C. R. and Nolan, T. A. Creep and stress rupture behavior of an advanced silicon nitride: Part 1, Experimental observations *J. Am. Ceram. Soc.* **77** 1994 1217–1227. Part II, Creep rate behavior. *J. Am. Ceram. Soc.*, **77**, 1994 1228–1234.
43. Rendtel, A., Hübner, H. and Herrmann, M., Creep behaviour of Si_3N_4/SiC-nanocomposite materials. In *Fourth Euro Ceramics. Basic Science — Trends in Emerging Materials and Applications*, Vol 4, ed. A. Bellosi. Gruppo Editoriale Faenza Editrice S.p.A., Faenza, Italy, 1995, pp. 225–232.
44. Wiederhorn, S. M., Hockey, B. J., Cranmer, D. C. and Yeckley, R., Transient creep behaviour of hot isostatically pressed silicon nitride. *J. Mater. Sci.*, 1993, **28**, 445–453.
45. Ohji, T. and Yamauchi, Y., Tensile creep and creep rupture behavior of monolithic and SiC-whisker-reinforced silicon nitride ceramics. *J. Am. Ceram. Soc.*, 1993, **76**, 3105–3112.
46. Nixon, R. D., Koester, D. A., Chevacharoenkul, S. and Davis, R. F., Steady-state creep of hot-pressed SiC whisker-reinforced silicon nitride. *Composites Science and Technology*, 1990, **37**, 313–328.